

A novel meso-mechanical model for concrete fracture

R. Ince[†]

Engineering Faculty, Civil Engineering Department, Firat University, Elazig, Turkey

(Received January 23, 2003, Accepted March 8, 2004)

Abstract. Concrete is a composite material and at meso-level, may be assumed to be composed of three phases: aggregate, mortar-matrix and aggregate-matrix interface. It is postulated herein that although non-linear material parameters are generally used to model this composite structure by finite element method, linear elastic fracture mechanics principles can be used for modelling at the meso level, if the properties of all three phases are known. For this reason, a novel meso-mechanical approach for concrete fracture which uses the composite material model with distributed-phase for elastic properties of phases and considers the size effect according to linear elastic fracture mechanics for strength properties of phases is presented in this paper. Consequently, the developed model needs two parameters such as compressive strength and maximum grain size of concrete. The model is applied to three most popular fracture mechanics approaches for concrete namely the two-parameter model, the effective crack model and the size effect model. It is concluded that the developed model well agrees with considered approaches.

Key words: concrete; fracture mechanics; numerical modelling; two-parameter model; effective crack model; size effect model.

1. Introduction

In material sciences, various scale classifications have been used in order to analyse the structures. However, the three-level approach is first proposed by Wittmann (1983) for cement based materials like concrete. Wittmann named these levels macro, meso, and micro. In the classification, each lower level includes more structural detail than its upper level. Concrete at the macro level is assumed as a homogeneous isotropic material. The meso level considers grain structures of concrete, cracks and voids. At this level, concrete is commonly modelled as a three-phase material: aggregate, cement paste (matrix) and aggregate-matrix interface which plays an important role in the non-linear behaviour of concrete. The micro level especially deals with hardened cement paste.

Early modelling studies on the concrete fracture were performed at the macro-level. Firstly, Smeared Crack Model, which was simulated the cracking in concrete structures in finite element analysis by adjustments of material stiffness, was proposed by Rashid (1968). This model was improved by de Borst (1984), Bazant (1986), de Borst (1987) and Rots (1988). Subsequently, another important macroscopic fracture models such as Fictitious Crack Model by Hillerborg *et al.* (1976), Crack Band Theory by Bazant and Oh (1983), and Damage Model by Mazars (1986) have been extensively used. In these models, non-linear analyses of concrete were performed by using

[†] Ph. D.

stress-strain relationship which includes behaviour of tension-softening of concrete. The necessity for too many parameters, to be known, which give different results according to boundary conditions and geometry of structures seems the most important disadvantage of these macroscopic models. These difficulties in the application of the macroscopic models have caused the development of the meso-mechanical approaches by directly simulating heterogeneous structure of concrete.

The meso-mechanical models have developed in two categories as continuum models and non-continuum models. The continuum models (Roelfstra 1988, Stankowsky 1990, Vonk *et al.* 1991, Wang *et al.* 1992, Kwan *et al.* 1999) simulate the heterogeneous structure of concrete by continuum finite elements while the non-continuum models simulate it by truss and beam elements. As a result, they are generally defined as lattice models in the literature (Bazant *et al.* 1990, Schlangen 1993, Mohamed and Hansen 1999, Arslan *et al.* 2002, Ince *et al.* 2003).

Non-linear material parameters were used in all of the meso-mechanical studies except Wang *et al.* (1992) and Schlangen (1993). However, Linear Elastic Fracture Mechanics (LEFM) principles can be used for modelling at the meso level (Reinhardt 1989, Ince 2001) if the properties of all three phases of concrete are known. This situation is not valid for macroscopic fracture models since cracks in concrete develop progressively. For instance, in a specimen subjected to tensile stresses, while cracks only develop in the interface phase at the low stresses level, these cracks penetrate into the matrix phase with increasing stresses and also collapse may occur in the aggregate phases at the high stresses level. Consequently, a macro crack in concrete occurs from resultant of several micro cracking stages. In this reason, the resultant of linear-elastic behaviour of each finite element at the meso-scale represents non-linear behaviour at the macro-scale in the comparison between macroscopic finite element and a meso-scale structure in the same scale which consist of several finite elements.

In this paper, a novel meso-mechanical continuum model in which the internal structure of concrete with three phases is implemented by using a generated grain structures in two dimensions is presented. The model is fundamentally established on a mechanical relation based on LEFM between macro-scale material parameters and meso-scale material parameters. In this respect, the model only needs two parameters such as compressive strength of concrete obtained from standard cylinders and maximum aggregate diameter of concrete. It is assumed that all elements in the model are linear-elastic and collapse under the tensile stresses. The composite material model with distributed-phase (Mindess and Young 1981) for elastic properties of elements and the theory of size effect based on LEFM for strength properties of phases are used in the presented model. The developed numerical model is tested by applying most popular approach in the fracture mechanics of concrete namely, Two Parameters Model (TPM) by Jenq and Shah (1985), Effective Crack model (ECM) by Karihaloo and Nallathambi (1986), Size Effect Model (SEM) by Bazant and Pfeiffer (1987), and energetic size effect formula by Bazant and Novak (2000). For this reason, several experimental studies in the literature (Bazant and Pfeiffer 1987, Nallathambi and Karihaloo 1989, Sabnis and Mirza 1979) are simulated by the model and it is found that the developed model well agrees with experimental and theoretical results.

2. Description of the model

2.1 Generation of grain structure

In the developed model, concrete is taken into consideration as a composite material with three

phases: course aggregate, mortar-matrix consist of fine aggregate and cement, and aggregate-matrix interface. The shape of aggregate particles is chosen as ellipse with maximum size/minimum size ratio ranging from 1 to 2, randomly. They are generated according to the Walraven's formula (1980), which is Fuller grading curve in two dimensions, as follows

$$P_c(D) = P_k \left[1.065 \left(\frac{D}{d_{\max}} \right)^{0.5} - 0.053 \left(\frac{D}{d_{\max}} \right)^4 - 0.012 \left(\frac{D}{d_{\max}} \right)^6 - 0.045 \left(\frac{D}{d_{\max}} \right)^8 + 0.025 \left(\frac{D}{d_{\max}} \right)^{10} \right] \quad (1)$$

in which D is the sieve size (the minimum size of ellipse in this study), $P_c(D)$ is the probability of the existence of an aggregate particle of size D , d_{\max} is the maximum aggregate size used in the simulation, and P_k is the aggregate volume fraction (P_k is usually 0.75). It is noted that more advanced studies for aggregate structures generation was performed by Wang *et al.* (1999).

The generated grain structure is randomly distributed from the large particles to the small particles in the specimen space. The minimum distance between two particle centres is taken $l_{\min} = 0.55(d_1 + d_2)$, where d_1 and d_2 are the sizes of the two particles (Hsu *et al.* 1963). Aggregates, the size of which are larger than $d_{\min} = 5$ mm, are generated in the model.

2.2 Mesh generation

In the developed model, Constant Strain Triangle (CST), which is the basic element of the

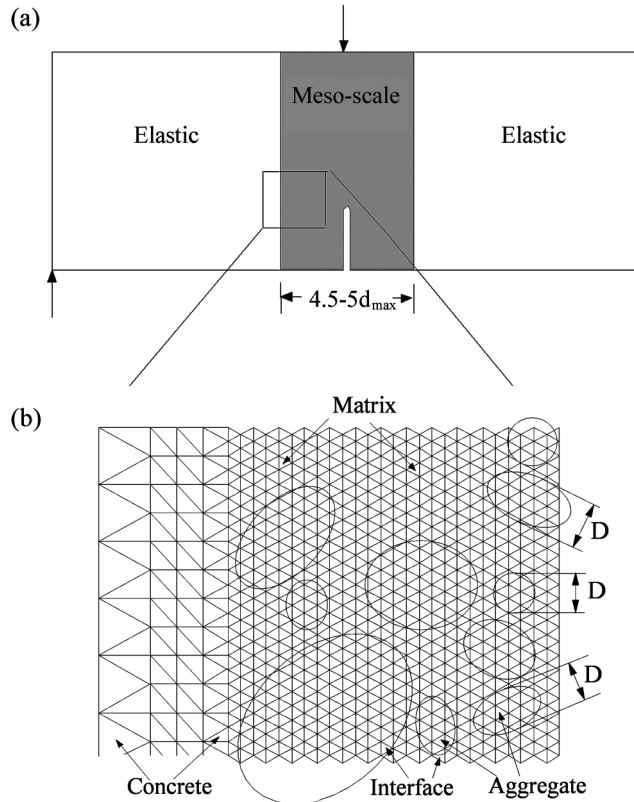


Fig. 1 Mesh generation and definition of aggregates, matrix, interface and concrete elements

continuum finite element, is used due to well simulation of the heterogeneous structure of concrete. As shown in Fig. 1, CST elements with different sizes are utilized to speed up the computations in a three-point bending specimen with a central edge notch. Small equilateral CST elements in the probable region of crack propagation and large non-equilateral CST elements in the remaining part of region are used for mesh generation. Only the middle portion of the specimen is simulated by using the meso-mechanical model, while the other parts are considered elastic. The width of the meso-level region is taken about 4.5-5.0 d_{\max} . This width is chosen as the width of the fracture process zone of concrete, which is approximately 2-4 d_{\max} (Bazant and Oh 1983). At the meso-level region, it is assigned aggregate element if all ends of an element fall in the aggregate phase. Then it is assigned matrix element if all ends of an element fall in the matrix phase and the other elements are assigned interface element. Elements in the remaining part are assigned concrete elements.

In the novel model, the length of element at the meso-level, which is equal to a side of element, is taken approximately one third of the minimum aggregate diameter used in the simulation like the lattice models (van Mier 1997). The thickness of elements is taken equal to the specimen thickness.

2.3 Assignment of material properties

2.3.1 Elastic properties

In the developed model, behaviours of materials for all phases are assumed to be linear-elastic. To determine the distribution of Young's modulus at the meso-scale region, the composite material model with distributed-phase is used as follows

$$E_C = \left[\frac{(1 - V_A)E_M + (1 + V_A)E_A}{(1 + V_A)E_M + (1 - V_A)E_A} \right] E_M \quad (2)$$

where E_C , E_M , E_A are the Young's modulus of concrete, matrix phase, and aggregate phase, respectively and V_A is the volume of aggregate (Mindess and Young 1981). In Eq. (2), Young's modulus of concrete is determined according to ACI-318 (1989) following by

$$E_C = 4734 \sqrt{f'_c} \text{ [MPa]} \quad (3)$$

in which f'_c is the compressive strength of the concrete. The Young's modulus of aggregate phase, E_A is taken 75 GPa in this study. This value is the median of Young's modulus of aggregate used in the concrete (van Mier 1997). The Young's modulus of matrix phase, E_M in the Eq. (2) is calculated by using the trial and error method from $V_A = n(A)/n(T)$, in which $n(A)$ and $n(T)$ are the number of aggregate elements and the number of total elements at the meso-scale region, respectively.

The Young's modulus of interface phase, E_B is taken as equal to the Young's modulus of matrix phase and the Poisson's ratio of all of phases, ν is taken as 0.2 in the developed model (van Mier 1997).

2.3.2 Strength properties

When the stress intensity factor K_I , in which is considered mode I, in the crack tip of notched specimens under the load reaches to the critical stress intensity factor K_{Ic} , the crack progresses as unstable according to LEFM. LEFM only appropriates for the problems with single crack which is isolated from the system. However, there are many micro cracks in addition to single macro crack in the notched concrete specimen at the meso-level. Therefore, it is difficult to use this form of LEFM

approach for concrete-like materials at the meso-level. For this reason, the size effect theory of LEFM is used to determine strength parameters of materials in the developed model.

In the LEFM, the critical stress intensity factor can be defined as

$$K_{Ic} = \sigma_N \sqrt{a_0} f(g, p) \quad \text{or} \quad K_{Ic} = \sigma_N \sqrt{d} f'(g, p) \quad (4)$$

where σ_N is the nominal strength, a_0 is the initial notch length, d is the characteristic dimension of specimen, chosen to coincide with the specimen depth, and $f(g, p)$ is a shape factor depending on the loading and specimen geometry. In Eq. (4), a relation-ship between the nominal strength and the characteristic dimension can be written as

$$\sigma_N = \frac{C}{\sqrt{d}} \quad (5)$$

in which C is a constant.

To determine the tensile strength of the matrix phases in the developed model, the results of experimental study on the notched direct tension specimens made of mortar by Bazant and Pfeiffer (1987) are used. They used a mortar with the compressive strength $f'_c = 47.6$ MPa, obtained from cylinder in a size of 76.2×152.4 mm, and with the maximum gravel size $d_{\max} = 4.83$ mm, in their study. The following values were used in the experiment: the width of all of the specimen $b = 19.05$ mm, the characteristic dimensions of the specimens $d = 38.1, 76.2,$ and 152.4 mm, the initial notch depth of the specimens $a_0 = d/6$, and the specimens length $L = 8/3d$ (Fig. 2a).

In the present paper, the nominal strengths are calculated at the notch level since $f(g, p)$ is approximately 1.12 for $a_0/d < 0.2$ in this type specimens ($\sigma_N = 2P_u/(3bd)$, where P_u is the maximum load. In this connection, the relation-ship between the nominal strength and the characteristic dimensions is obtained with normalized values for LEFM as follows (see Eq. (16))

$$\sigma_N = 1.493 f'_t \sqrt{\frac{20.59 d_{\max}}{d}} \quad (6)$$

in which f'_t is the tensile strength of the material and can be determined according to ACI-318 (1989) by

$$f'_t = 0.4983 \sqrt{f'_c} \quad [\text{MPa}] \quad (7)$$

Indeed, the matrix phase is a composite material since of including aggregates smaller than 5 mm in size. To display the consequences of heterogeneity of the matrix phase correctly, d in Eq. (6) can not be less than three maximum aggregate size, as shown in Fig. 2(b), because the material could no longer be continuous (Bazant and Novak 2000). As a result of this, the relation-ship between macro-scale (laboratory scale) and meso-scale is obtained from Eq. (6) as

$$f_t^M = 3.91 f_t'^M \quad (8)$$

where f_t^M is the tensile strength used the simulation of the matrix phase (meso scale), and $f_t'^M$ is the tensile strength obtained from standard cylinder with a size of 150×300 mm (laboratory scale). $f_t'^M$ in Eq. (8) can be calculated from Eqs. (3) and (7) as follows

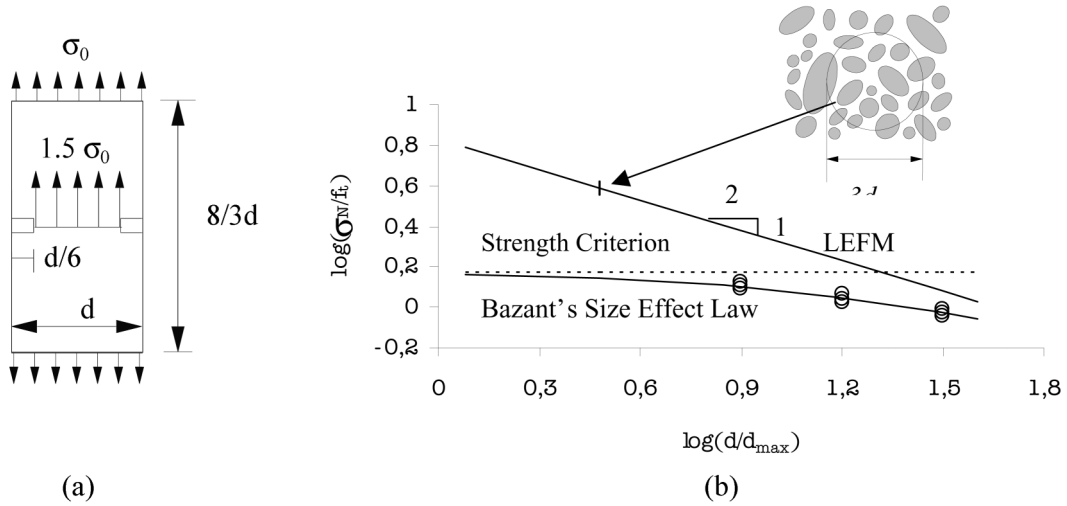


Fig. 2 Determination of the relation-ship between meso scale and laboratory scale for matrix phase (a) the direct tension specimen configuration used the analysis (Bazant and Pfeiffer 1987) (b) the size effect diagrams according to Bazant's size effect law and LEFM

$$f_t'^M = 1.05 \cdot 10^{-4} E_M \quad (9)$$

The experimental studies point out that the tensile strength of the interface phase is 33 to 67% of the tensile strength of the matrix phase (Huang and Li 1989). In the novel model, this value is taken as 35%, which is near the lower limit, because of modelling in two dimensions and also by considering effect of third dimension. The tensile strength of the aggregate phase is taken as 25 MPa.

2.4 Constitutive matrix

It is shown in Fig. 3 that the constitutive matrix of elements is arranged in four cases considering crack forming of the element. In the Case I, the constitutive matrix of the uncracked element can be expressed by

$$D_e = \frac{E}{(1-\nu^2)} \begin{bmatrix} 1 & \nu & 0 \\ \nu & 1 & 0 \\ 0 & 0 & (1-\nu)/2 \end{bmatrix} \quad (10)$$

in which E and ν are the Young's modulus and The Poission's ratio of the element, respectively. An element with single crack is represented in the Case II. In the case, it is assumed that the material cannot sustain any tensile stress towards the normal direction of the crack. Therefore, the orthotropic constitutive matrix is used in the case, in which The Young's modulus towards the normal direction of the crack is equal to zero and the Young's modulus towards the tangent direction of the crack is equal to the Young's modulus of the material. Hence,

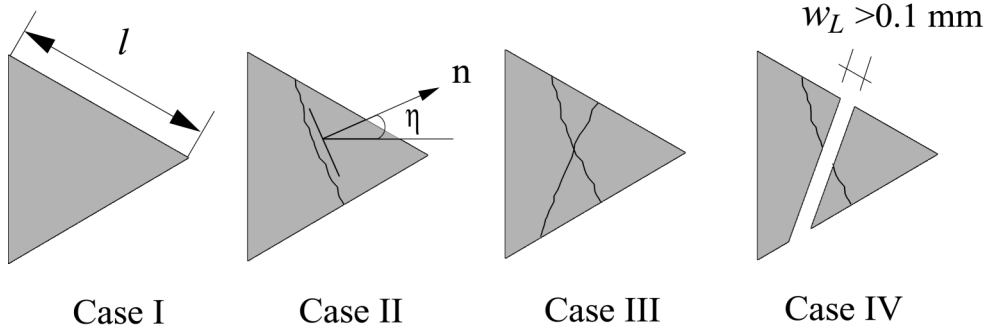


Fig. 3 The element cases in the developed model

$$D_e = \begin{bmatrix} 0 & 0 & 0 \\ 0 & E & 0 \\ 0 & 0 & \beta G \end{bmatrix} \quad (11)$$

where β is the shear retention factor ($0 \leq \beta \leq 1$), which satisfies transferring the shear stresses to the cracked section and reduces the numerical difficulties, and G is the shear modulus ($G = E/2(1 + \nu)$). β is taken 0.03 for the Case II in the developed model. However, the constitutive matrix in Eq. (11) is current in the local coordinate system. So, it must be transformed from the local coordinate system aligned with the crack to the global coordinate system as follows

$$D_n = T^T D_e T \quad (12)$$

in which T is the transformation matrix as

$$T = \begin{bmatrix} c^2 & s^2 & cs \\ s^2 & c^2 & -cs \\ -2cs & 2cs & c^2 - s^2 \end{bmatrix} \quad (13)$$

where $c = \cos\eta$, $s = \sin\eta$, and η is the angle between the local x axis and the normal direction of the crack.

In the Case III, an element with non-parallel double cracks is represented as follows, in which is only assumed to transferring the shear stresses on the surface of the cracks.

$$D_e = \begin{bmatrix} 0 & 0 & 0 \\ 0 & 0 & 0 \\ 0 & 0 & \beta G \end{bmatrix} \quad (14)$$

In the last case, it is assumed that the crack width in the element is too large to permit transferring the shear stress. In the present study, the limit crack width is taken 0.1 mm because of modelling at the meso level. The constitutive matrix in the Case IV is the same as Eq. (14), but the shear retention factor, β is taken 1e-10 for eliminating the probable singularities in the global stiffness matrix. In this paper, the fractured element is defined as the element with double cracks (Case III).

3. Validation checks

The validity of the proposed numerical model was checked by simulating the experimental studies, all of which were made to determine non-linear fracture parameters of concrete by using the different fracture models, (1) by Nallathambi and Karihaloo (1989) for TPM and ECM, and (2) by Bazant and Pfeiffer (1987) for SEM. Three-point bending specimens with a central edge notch were used in all of the above experimental studies. In addition, the developed numerical model was checked by simulating the unnotched beams of different size by Sabnis and Mirza (1979).

3.1 Application to the TPM and ECM

It is assumed that the initial crack length a_0 in Eq. (4) according to LEFM does not change until reaching the maximum load. However, the crack reaches the critical length and starts to progress in an unstable way when the peak load is exceeded. The crack also develops in a stable manner until the peak load is reached since the size of the fracture process zone can be relatively larger than the specimen size in the concrete-like quasi-brittle materials. Consequently, the critical crack length, a_e must be considered in the evaluation of K_{Ic} in Eq. (4) for concrete.

Two methods have been commonly used in order to define this non-linear behaviour (Jenq and Shah 1985, Karihaloo and Nallathambi 1986). TPM approach uses two parameters such as the critical stress intensity factor K_{Ic}^s and the critical crack tip opening displacement $CTOD_c$ for modelling of concrete fracture. The approach calculates these parameters from relationship P-CMOD of specimens by using a closed-loop test equipment. a_e in TPM is determined from two values measured on P-CMOD curve viz., the initial compliance (C_i) and the unloading compliance (C_u) measured at about 95% of the peak load after the peak load (Fig. 4a). ECM approach is similar in concept to the TPM approach and includes parameters such as the critical stress intensity factor K_{Ic}^e and the effective crack length a_e to characterize failure of concrete structures. The approach benefits from relationship P- δ of the specimens to calculate these parameters. Both TPM and ECM generally use three point bending beams with a central edge notch. The theoretical details of TPM and ECM are given in Appendix A and B, respectively.

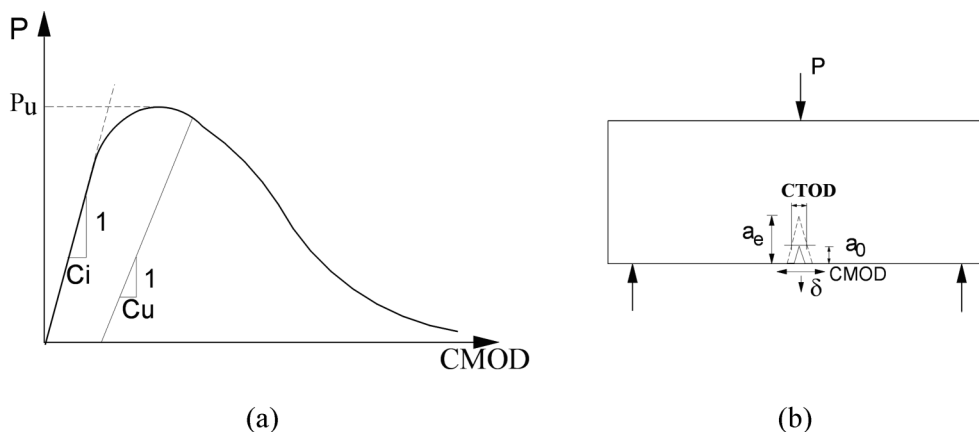


Fig. 4 Determination fracture parameters according to TPM and ECM (a) typical P-CMOD curves for TPM (b) measure values

Table 1 The mean material parameters for the application of TPM and ECM

Mix	Parameter	Concrete	Matrix (sd)	Bond (sd)
C1 $f'_c = 26.8$ MPa	E [GPa]	24.51	16.85 (0.33)	16.85 (0.33)
	f'_t [MPa]	-	6.92 (0.14)	2.42 (0.04)
C2 $f'_c = 39.0$ MPa	E [GPa]	29.56	21.46 (0.09)	21.46 (0.09)
	f'_t [MPa]	-	8.82 (0.02)	3.08 (0.01)
C3 $f'_c = 49.4$ MPa	E [GPa]	33.27	24.92 (0.15)	24.92 (0.15)
	f'_t [MPa]	-	10.23 (0.06)	3.58 (0.02)

sd = standard deviation

The experimental study which is carried out to compare TPM and ECM approaches by Nallathambi and Karihaloo (1989) is used for numerical application in this study. Three standard $80 \times 200 \times 800$ mm beams were produced from five different concrete mix (C1, C2, C3, C4 and C5) with the compressive strength from about 25 MPa to nearly 80 MPa and $d_{\max} = 20$ mm. The ratios of lengths of notches to the depths of beams were 0.3. All of the specimens were tested with the CMOD controlled machine.

In this paper, the specimens with $f'_c < 50$ MPa (normal concrete: C1, C2 and C3) were simulated. Three specimens were created for each of the mix. The aggregates from 5 mm to 20 mm in size were distributed to the space of the simulated specimens, randomly. Lengths of the elements were chosen $l = 1.5625$ mm and totally 23278 finite elements were used so as to simulate the experimental specimens. The evaluated mean material parameters of each mix are given in Table 1.

The specimens were simulated CMOD controlled. The predicted vertical displacement at the notch level, the load and values of CMOD and CTOD which were measured from the horizontal displacements of the two nodes at the corners of the notch at its mouth and tip, respectively were saved in each of the iteration (Fig. 4b). The plots of P- δ , P-CMOD and P-CTOD for the first series of each mix (C11, C21 and C31) are shown in Figs. 5(a-c). The calculated fracture parameters of the experimental and simulated specimens according to TPM and ECM are shown in Table 2. The value of the C_u in TPM is directly evaluated from $0.95P_u/\text{CMOD}$ since LEFM principles are used in this study. However, this is a highly realistic approach, because the values of calculated E'_{TPM} using C_u in Table 2 are quite close to E_{TPM} values. The overall error between the experimental results and the prediction of the model in Table 2 is obtained as 8.4%.

The crack patterns of C11, C21 and C31 specimens at the peak load are given in Fig. 6 to compare with the calculated critical crack lengths of the experimental and the simulated specimens according to TPM and ECM approaches given in Table 2. The relation between CTOD and cumulative number of fractured elements of the C11, C21 and C31 specimens is given in Fig. 7 to obtain numerical initiation of unstable crack progression. Consequently, the fact that the relation has a severe slope before 0.025 mm value and then has a slight slope as shown in Fig. 7. Both Fig. 6 and Fig. 7 indicate that the calculated fracture parameters in Table 2 and the measured ones in the simulated specimen agree with each other.

By way of an example, the simulation of the C11 specimen will be discussed in detail. The P-CMOD curve of this specimen is shown in Fig. 8 on which are identified eight points with numbers from 1 to 8 for closer examination. The fracture state and stress distribution through the cross section at midspan at each of the identified points are separately recorded in Figs. 9(a-h). It gives a

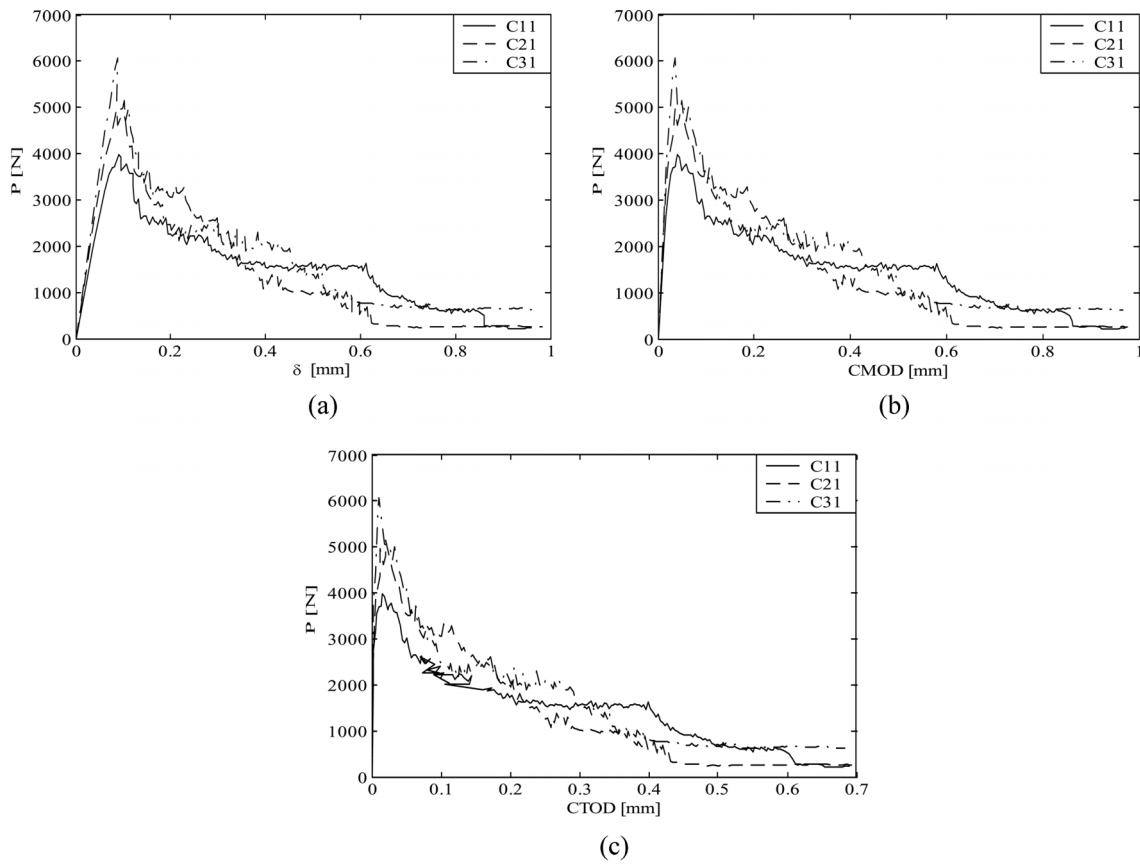


Fig. 5 Predicted (a) P- δ (b) P-CMOD (c) P-CTOD curves for C11, C21 and C31 simulated specimens

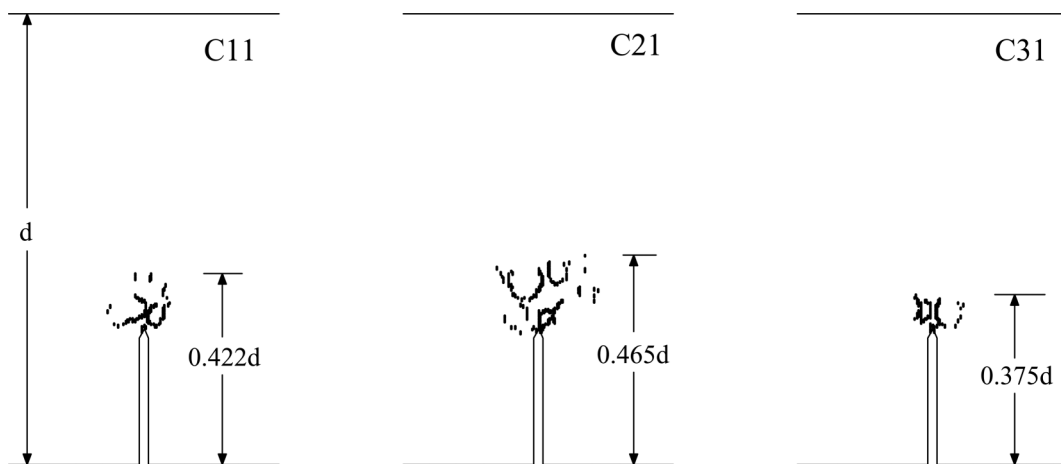


Fig. 6 Crack pattern at the peak load for the first specimen of each series

close view of the region extending on either side of the notch over the entire depth of the beam. The positions of the fractured elements are shown in the figures together with the load level, and the

Table 2 The comparison with the experimental and the numerical fracture parameters for the application of TPM and ECM

Fracture Parameters	Experimental			Numerical		
	C1	C2	C3	C1	C2	C3
	Mean(sd)	Mean(sd)	Mean(sd)	Mean(sd)	Mean(sd)	Mean(sd)
E_{TPM}	24.04(.29)	31.56(.64)	32.96(.24)	24.05(.55)	29.11(.24)	32.88(.35)
E'_{TPM}	-	-	-	23.65(.53)	29.04(.25)	32.60(.25)
a_c/d	0.443(.015)	0.442(.006)	0.436(.001)	0.419(.018)	0.446(.005)	0.415(.012)
K_{Ic}^s	0.993(.054)	1.269(.028)	1.381(.031)	0.952(.050)	1.278(.028)	1.364(.220)
$CTOD_c$	0.033(.010)	0.026(.001)	0.026(.001)	0.022(.002)	0.028(-)	0.023(.007)
E_{ECM}	25.56(.35)	29.87(.21)	33.28(.22)	25.44(.32)	30.72(.15)	34.63(.04)
a_c/d^1	0.447(.003)	0.454(.001)	0.446(.003)	0.418(.023)	0.443(.007)	0.398(.032)
a_c/d^2	0.443(.150)	0.442(.006)	0.436(.001)	0.452(.007)	0.449(.004)	0.448(.004)
K_{Ic}^e	0.992(.015)	1.265(.013)	1.376(.020)	0.947(.035)	1.268(.103)	1.300(.210)

a_c/d^1 and a_c/d^2 are calculated from Eq. (26) and Eq. (27), respectively
 E in [GPa], K_{Ic} in [MPa√m] and $CTOD_c$ in [mm]

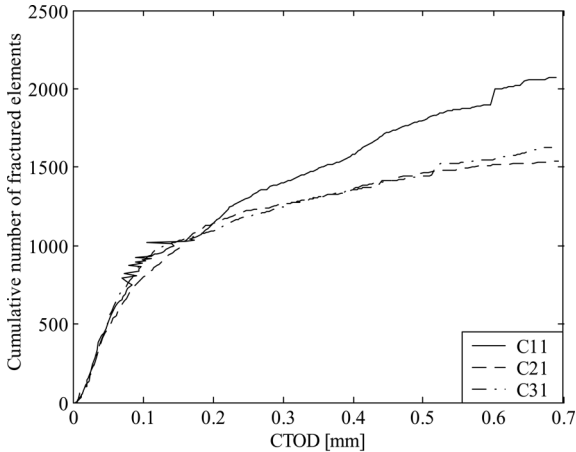


Fig. 7 Variation of number of fractured elements versus CTOD for the first specimen of each series

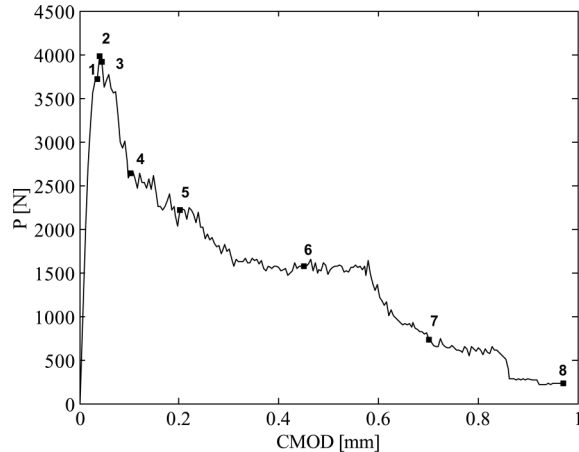


Fig. 8 Chosen eight plot in P-CMOD of C11 specimen

numbers of fractured aggregates (A), interface (I), matrix (M) elements, width of cracked zone (w_c) and length of cracked zone (l_c) at this load level. These traces are useful in following the fracture process in the specimen.

Before the peak load is reached, the cracks are mainly observed in the interface phase of the specimen; the number of matrix cracks is only 5% of the total number of cracks. As the number of cracks is small in the dominant (matrix) phase of concrete, the specimen continues to carry more load (i.e., to harden). There is no coalescence or branching or localization of cracks (see Fig. 9a). At the peak load ($P = 3980$ N), the microcracks spread over a slightly wider area, with an increase

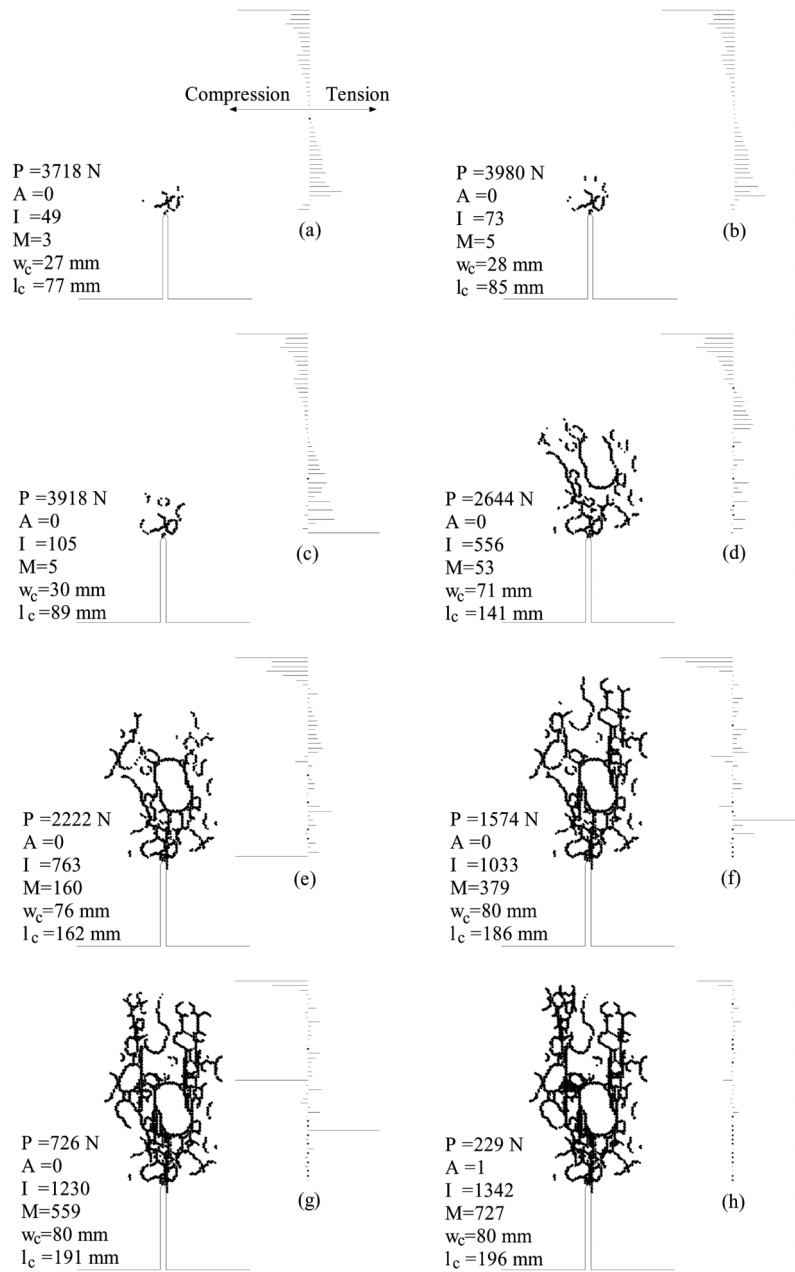


Fig. 9 Stress distribution along the depth at midspan, in specimen C11, at eight points (a-h) of P-CMOD diagram (Fig. 8). Also shown are microcracking, crack coalescence and branching at the eight load levels

in the number of fractured matrix elements; it is now over 7% of the interface elements, but there is no major change in the stress distribution through the depth of the beam. However, immediately past the peak load (Fig. 9c-e) the tensile stress ahead of the notch changes dramatically, and the size of

the compression zone decreases. There is a noticeable discontinuity in the tensile stresses ahead of the notch tip. The cracks localize along the depth at midspan as the number of fractured matrix elements dramatically increases up to almost 17% of the fractured interface elements. As the load decreases, more and matrix elements are fractured, the cracks branch, the fracture process zone widens, the tensile stress decreases, and the neutral axis shifts upwards. The final trace at point 8 (Fig. 9h) clearly shows that the specimen load carrying capacity is due to aggregate interlock and bridging only.

3.2 Application to SEM

Many experimental investigations indicate that the nominal strength (σ_N) decreases with increasing specimen size (d) for the geometrically similar specimens. This phenomenon is called the size effect. Bazant (1983, 1987) defined the relationship between σ_N and d which is called Size Effect Law (SEL) as follows

$$\sigma_N = \frac{Bf'_t}{\sqrt{1 + \beta}}, \quad \beta = \frac{d}{\lambda_0 d_{\max}} \quad (15)$$

in which B and λ_0 are the empirical constants. These constants can be calculated as $B = 1/\sqrt{C}$ and $\lambda_0 = C/A$ from the linear regression made on $Y = AX + C$ with $Y = (f'_t/\sigma_N)^2$, $X = d/d_{\max}$. β in Eq. (15) is the brittleness number and determine failure stage of specimen. The strength criteria is valid in case $\beta \rightarrow 0$, while failure is governed by LEFM criteria in case $\beta \rightarrow \infty$ given in the following

$$\sigma_N = Bf'_t \sqrt{\frac{\lambda_0 d_{\max}}{d}} \quad (16)$$

SEM approach introduces fracture parameters for an infinitely large specimen such as the fracture energy G_f , the effective fracture process zone length c_f , the critical stress intensity factor K_{Ic} , and the critical crack tip opening displacement δ_c , those of which calculated from above constants. The details for calculation of the fracture parameters are given in Appendix C.

The experimental study performed to investigate the size effect in three point bending beams by Bazant and Pfeiffer (1989) is simulated in this study. They tested four geometrically similar, notched three-point bend specimens of varying depths as follows: $d = 38.1$ mm small (S), 76.2 mm medium (M), 152.4 mm large (L), and 304.8 mm huge (H). In all beams the width $b = 38.1$ mm, length to depth ratio $L/d = 8/3$, loaded span to depth ratio $S/d = 2.5$ and notch depth $a_0 = d/6$ were the same. The material parameters needed in the numerical model were: the maximum size of coarse aggregate $d_{\max} = 12.7$ mm and $f'_c = 33.5$ MPa, which is determined from cylinder with 76.2×152.4 mm.

In order to simulate the behaviour due to the random distribution of the aggregates, three different granular distributions were used for each specimen geometry. The granular distribution is chosen according to Eq. (1) with the grains between 5 mm (4.83 mm) and 13 mm (12.7 mm). The element length at the meso-scale region in the simulation was chosen as $l = 1.5875$ mm. Consequently, 1898 finite elements were used for small, 5462 for medium, 12414 for large and 30642 for huge in order to simulate the experimental specimens. The material parameters were: E of matrix phase and interface phase = 20.99 (0.69) GPa and f'_t for phases of matrix and interface = 8.62 (0.28) MPa and 3.02 (0.10) MPa, respectively, in which the values in the parenthesis indicate the standard deviations.

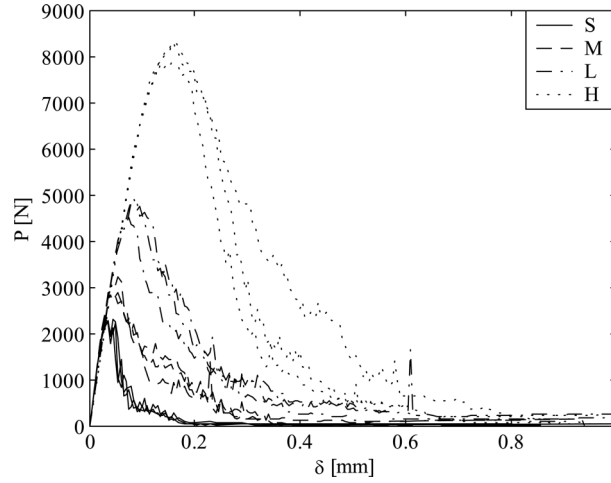


Fig. 10 Simulated P- δ relationships for small, medium, large and huge specimens

Table 3 The comparison with the experimental and the numerical maximum load

Type	P_u^{num} [N]			Mean P_u^{num} [N] (sd)	Mean P_u^{exp} [N] (sd)
	1	2	3		
<i>S</i>	2293	2241	2297	2277 (26)	1820 (26)
<i>M</i>	3230	2824	2909	2988 (175)	3103 (81)
<i>L</i>	4511	4942	4844	4766 (185)	4637 (240)
<i>H</i>	7851	8316	8300	8156 (216)	7787 (90)

The predicted P- δ curves of the Small, Medium, Large and Huge specimens are shown in Fig. 10, respectively. The displacements given in the figures are measured at the load application point. The experimental and numerical maximum mean loads are given for each specimen in Table 3.

Table 3 shows that a great deal of error occurs between experimental and numerical maximum loads for the small specimens. To explain the cause of the observed errors, the crack patterns at the failure of S1, M1, L1 and H1 specimens were investigated as shown in Fig. 11. It is shown that the crack band width of S1 specimen is $1.73d_{max}$ and the 54% of the number of the fractured elements are interface elements, while the crack band width of H1 specimen is $5.22d_{max}$ and the 67% of the number of the fractured elements are interface elements. Hence, it may be obtained a result of the fact that space of S type specimens is not as large as to assure suitable aggregate distribution.

The estimated empirical constants, the correlation coefficients (r), the variation coefficient ($\omega_{Y/X}$), and the relative width of scatter-band (m) according to SEM approach are shown for the numerical and the experimental results in linear regression plots in Fig. 12(a). The comparative relation of the σ_N versus d and the fracture parameters of SEM approach obtained from the experimental and numerical results are given in Fig. 12(b) in the bilogarithmic plane. The overall error between the experimental results and the prediction of the model in Fig. 12(b) is obtained as 5.1%.

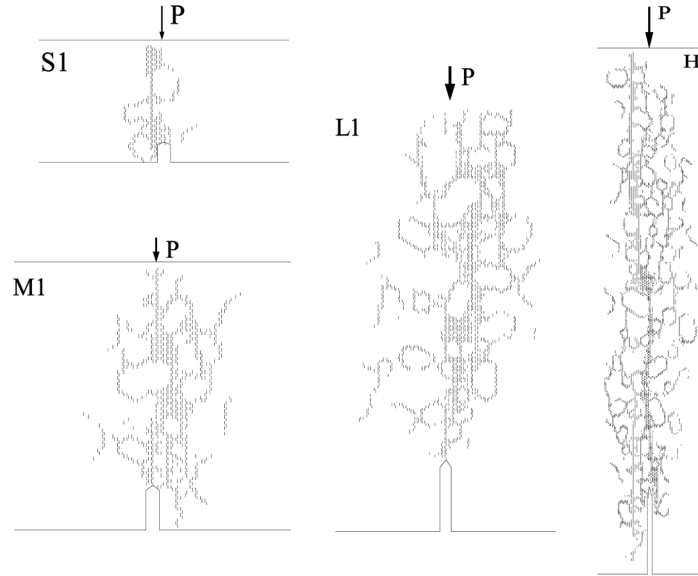


Fig. 11 Crack patterns at the failure stage for the first specimen of each series

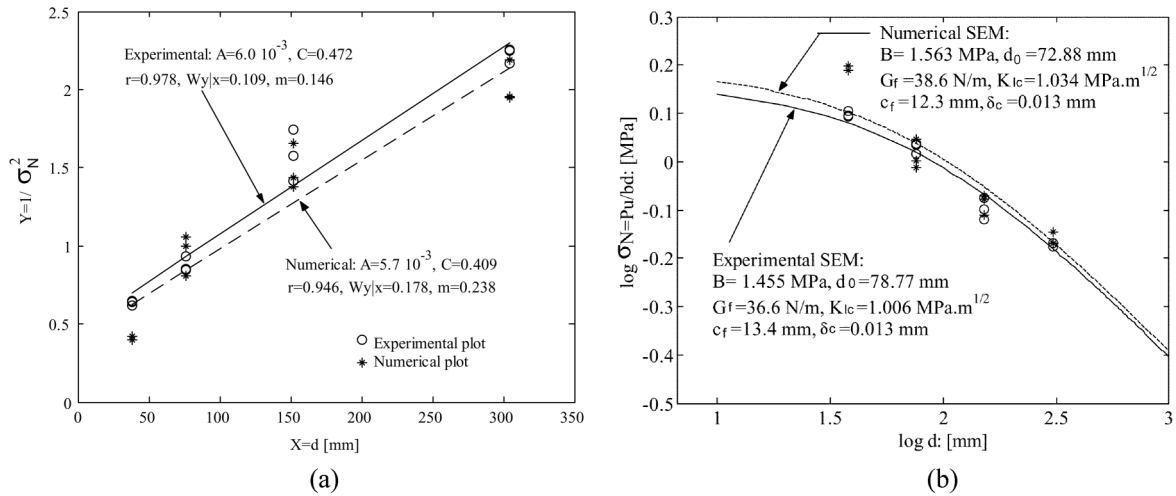


Fig. 12 Comparison of numerical nominal strength with experimental results according to Bazant's size effect law. (a) linear regression plot (b) size effect plot

3.3 Application to Bazant's energetic size effect formula

The flexural strength of concrete beams, known as the modulus of rupture, has been experimentally investigated by many researchers (Bazant and Novak 2000). The tests revealed that the rupture modulus decreases with increasing beam size. Bazant proposed the relationship between the rupture modulus f_r and d which is called the energetic-size effect formula as follows:

$$f_r = f_{r,\infty} r \sqrt{1 + \frac{r D_b}{d}} \quad (17)$$

in which $f_{r,\infty}$, r and D_b are the positive constants. These constants can be determined by a nonlinear optimization algorithm.

In this work, the experimental study by Sabnis and Mirza (1979) is modelled. They tested five geometrically similar unnotched four point bend specimens of varying depths as follow: $d = 9.53$, 19.1, 38.1, 76.2 and 152.4 mm. Each beam presented the width $b = 2/3d$, span/depth ratio $S/d = 4$ and tested in flexure in third-point loading. The material parameters are the following $E = 30$ GPa and $d_{\max} = 12.7$ mm.

Although no statistic about the number of test specimens for each depth was reported in the literature, three specimens were created for each of the size in this study. The aggregates from 5 mm to 13 mm in size were distributed randomly to the space of the simulated specimens. But, the aggregate distribution could not be obtained in the smallest specimen since its depth (9.53 mm) is smaller than the maximum aggregate size (12.7 mm). The element length at the meso-scale region with width about $S/3 + 3d_{\max}$ was chosen as $l = 1.5875$ mm. Consequently, 40938 finite elements were used for the largest specimen size. The material parameters were: E of matrix phase and interface phase = 25.44 (1.52) GPa and f'_t for phases of matrix and interface = 10.48 (0.62) MPa and 3.65 (0.22) MPa, respectively, in which the values in the parenthesis indicate the standard deviations.

The predicted P - δ curves for the first specimen of each specimen size are shown in Fig. 13. In this figure, the displacement values of the specimens are plotted until the displacement values were 0.21 mm since only the peak load values of specimens are necessary for the size effect analysis. The displacements given in the figure are measured at the load application points. Fig. 14 illustrates crack patterns at the displacement value = 0.21 mm for the first specimen of three largest specimen sizes. The comparative relation f_r versus d according to energetic-size effect formula are given in Fig. 15, in the bilogarithmic plane, for results of the experimental, the numerical and Bazant's

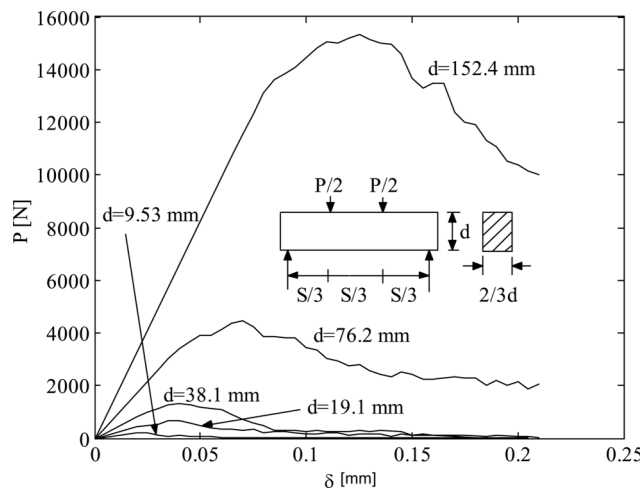


Fig. 13 Simulated P - δ relationships of specimens for the first specimen of each specimen sizes

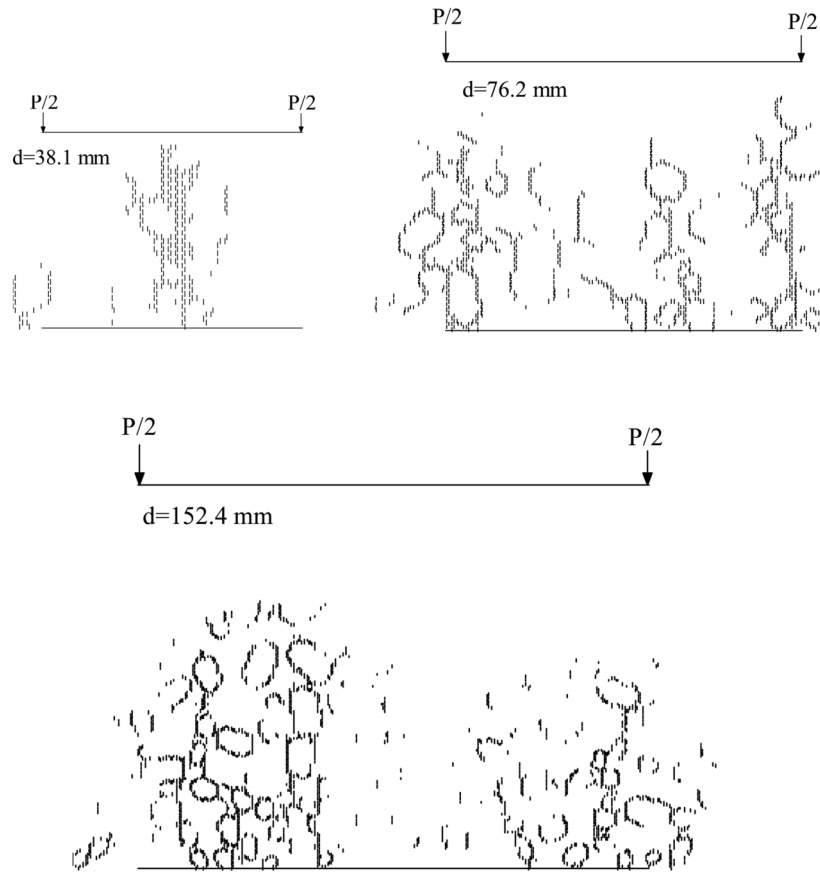


Fig. 14 Crack patterns at the displacement value = 0.21 mm for the first specimen of three largest specimen sizes

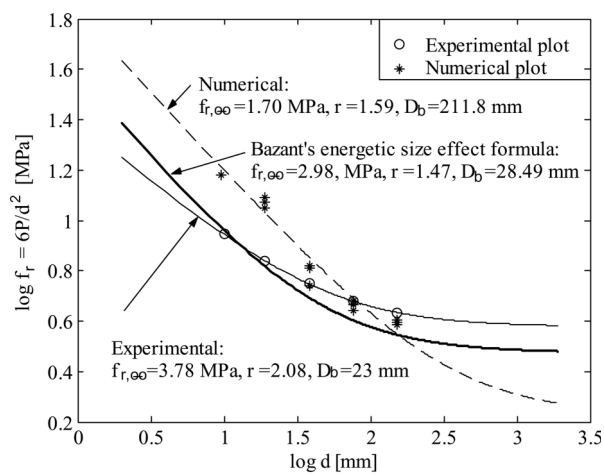


Fig. 15 Comparison of numerical nominal strength with experimental results according to Bazant's energetic size effect formula

approach that is obtained from data of the eight experimental investigations. The Levenberg-Marquardt nonlinear optimization algorithm was used to calculate the empirical constants in Eq. (17) in this study. It is shown in Fig. 15 that a great deal of error occurs between the experimental and the numerical rupture modulus for two smallest specimen sizes since spaces of these specimens are not as large as to assure suitable aggregate distribution.

4. Conclusions

In this paper, a novel continuum meso-mechanical model is developed and validated for fracture of concrete structures. The following conclusions can be drawn:

1. In the result of the simulations, although the developed model is only needed two parameters namely the maximum aggregate size and the compressive strength of concrete, which are most important two material parameters on the fracture parameters of concrete, it is shown that the presented model has an adequate approximation in the prediction of the fracture parameters of concrete, viz. the fracture energy, the effective crack length, the critical stress intensity factor and the critical crack tip opening displacement. This result brought up the fact that linear-elastic material parameters can be used in the meso-mechanical model although the non-linear material parameters must be used in the macroscopic models.
2. The applications indicate that the developed model has obtained the similar results with experimental investigations for stages of crack development and crack distribution band width. Besides, the predicted stress distribution on the notch of the simulated specimens well agrees with the stress distribution in the cohesive crack concept.
3. The most important difference of the novel model from the other models which uses linear-elastic material parameters has provided an adequate approximation in both predictions of the crack patterns and explanation of mechanical behaviour of specimens under loading. Two factors are to be efficient in providing of this situation: the first is the composite material model with distributed-phase found suitable for nature of concrete for elastic properties of phases, the second is size effect considered according to LEFM for strength properties of phases.
4. In comparison with the meso-mechanical model and the macroscopic model, the most important disadvantage of the first one is to necessitate too many finite elements in order to simulate any structure with the same scale. For example: in this study, 40938 finite elements were used for four point bending specimen with $d = 152.4$ mm, $S = 609.6$ mm.

References

- ACI-318 (1989), Building Code Requirements for Reinforced Concrete, Detroit.
- Arslan, A., Ince, R. and Karihaloo, B.L. (2002), "Improved lattice model for concrete fracture", *J. Eng. Mech.*, ASCE, **128**(1), 57-65.
- Bazant, Z.P. (1986), "Mechanics of distributed cracking", *Appl. Eng. Review*, ASME, **39**(5), 675-705.
- Bazant, Z.P. and Novak, D. (2000), "Energetic-statistical size effect in quasibrittle failure at crack initiation", *ACI Mat. J.*, **97**(3), 381-392.
- Bazant, Z.P. and Oh, B.H. (1983), "Crack band theory for fracture concrete", *Mat. Struct.*, **16**, 155-157.
- Bazant, Z.P. and Pfeiffer, P.A. (1987), "Determination of fracture energy properties from size effect and

- brittleness number”, *ACI Mat. J.*, **84**(6), 463-480.
- Bazant, Z.P., Tabbara, M.R., Kazemi, M.T. and Pijaudier-Cabot, G. (1990), “Random particle model for fracture of aggregate or fibre composites”, *J. Eng. Mech.*, ASCE, **116**(8), 1686-1705.
- de Borst, R. (1984), “Application of advanced solution techniques to concrete cracking and non-associated plasticity”, *Numerical Methods for Non-linear Problems*, Ed. Taylor, C. *et al.*, **2**, Pineridge Press, Swansea.
- De Borst, R. (1987), “Smearred cracking, plasticity, creep and thermal loading- a unified approach”, *Comput. Meth. Appl. Mech. Eng.*, **62**, 89-110.
- Hillerborg, A., Modeer, M. and Petersson, P.E. (1976), “Analysis of crack formation and crack growth in concrete by means of fracture mechanics and finite elements”, *Cement Conc. Res.*, **6**, 773-782.
- Hsu, T.T.C., Slate, F., Sturman, G. and Winter, G. (1963), “Microcracking of plain concrete and the shape of the stress-strain curve”, *J. American Conc. Ins.*, **60**, 209-224.
- Huang, J. and Li, V.C. (1989), “A meso-mechanical model of the tensile behaviour of concrete. Part I: modelling of the pre-peak stress-strain relation”, *Composites*, **20**(4), 361-369.
- Ince, R. (2001), “A new lattice model for concrete fracture at the meso level”, *Proc. XII National Mechanics Congress*, Konya, Turkey, September. (in Turkish)
- Ince, R., Arslan, A. and Karihaloo, B.L. (2003), “Lattice modelling of size effect in concrete strength”, *Eng. Frac. Mech.*, **70**, 2307-2320.
- Jenq, Y.S. and Shah, S.P. (1985), “A two parameter fracture model for concrete”, *J. Eng. Mech.*, ASCE, **110**(10), 1227-1241.
- Karihaloo, B.L. and Nallathambi, P. (1986), “Determination of specimen-size independent fracture toughness of plain concrete”, *Magazine Conc. Res.*, **38**(135), 67-76.
- Mindess, S. and Young, J.F. (1981), *Concrete*, Prentice-Hall, Inc., New Jersey.
- Kwan, A.K.H., Wang, Z.M. and Chan, H.C. (1999), “Mesoscopic study of concrete II: nonlinear finite element analysis”, *Comput. Struct.*, **70**, 545-556.
- Mazars, J. (1986), “A Description of micro and macro-scale damage of concrete structures”, *J. Eng. Frac. Mech.*, **25**(5/6), 729-737.
- Mohamed, A.R. and Hansen, W. (1999), “Micromechanical modelling of concrete response under static loading- Part I: Model development and validation”, *ACI Mat. J.*, **96**(2), 196-203.
- Nallathambi, P. and Karihaloo, B.L. (1989), “Fracture toughness of plain concrete from three-point bend specimens”, *Mat. Struct.*, **22**, 185-193.
- Rashid, Y.R. (1968), “Analysis of prestressed concrete pressure vessels”, *Nuclear Engineering and Design*, **7**(4), 334-355.
- Reinhardt, H.W. (1989), “Basic types of failure”, *Fracture Mechanics of Concrete Structure: From Theory to Applications* (Report of RILEM FMA-90), Ed. Elfgrén, L., Chapman & Hall, London.
- Roelfstra, P.E. (1988), “Simulation of strain localization process with numerical concrete”, *Proc. 'Cracking and Damage: Strain Localization and Size Effect*, Cachan, October.
- Rots, J.G. (1988), “Computational modelling of concrete fracture”, Dissertation, Delft University of Technology, The Netherlands.
- Sabnis, G.M. and Mirza, S.M. (1979), “Size effect in model concretes?”, *J. Struct. Div.*, ASCE, **106**, 1007-1020.
- Schlangen, E. (1993), “Experimental and numerical analysis of fracture processes in concrete”, Ph.D. Thesis. Delft University of Technology, The Netherlands.
- Stankowsky, T. (1990), “Numerical simulation of progressive failure in particle composites”, Ph.D Thesis, University of Colorado, USA.
- van Mier, J.G.M. (1997), *Fracture Processes of Concrete Assessment of Material Parameters for Fracture Models*, CRC Press, New York.
- Vonk, R.A., Rutten, H.S., Van Mier, J.G.M. and Fijneman, H.J. (1991) “Micromechanical simulation of concrete softening”, *Proc. 'Fracture Processes in Concrete*, Rock and Ceramics Congress, Noordwijk, June.
- Walraven, J.C. (1980), “Aggregate interlock: a theoretical and experimental analysis”, Ph.D. thesis, Delft University of Technology, The Netherlands.
- Wang, J., Navi, P. and Huet, C. (1992), “Numerical study of granule influences on the crack propagation in concrete”, *Proc. '1st Congress on Fracture of Concrete Structures*, Breckenridge, June.

- Wang, Z.M., Kwan, A.K.H. and Chan, H.C. (1999), "Mesoscopic study of concrete I: generation of random aggregate structure and finite element mesh", *Comput. Struct.*, **70**, 533-544.
- Wittmann, F.H. (1983), "Structure of concrete with respect to crack formation", *Fracture Mechanics of Concrete*, (Report of RILEM FMA-50), Ed. Wittmann, F.H., Elsevier, Amsterdam.

Appendix A

The calculation of the fracture parameters in TPM

The modulus of elasticity is calculated from the equations

$$E = \frac{6Sa_0V_1(\alpha_0)}{C_i b d^2} \quad (18)$$

$$V_1(\alpha) = 0.76 - 2.28\alpha + 3.87\alpha^2 - 2.04\alpha^3 \frac{0.66}{(1-\alpha)^2}, \quad S/d = 4 \quad (19)$$

where S is the loaded span, b is the thickness, d is the height, $\alpha_0 = a_0/d$ and C_i the initial compliance. However, E in Eq. (18) can be also evaluated from C_u the unloading compliance at 95% of peak load and $\alpha_e = a_e/d$. The effective crack length can be calculated by trial and error method as follows

$$a_e = a_0 \frac{C_u V_1(\alpha_0)}{C_i V_1(\alpha_e)} \quad (20)$$

The critical stress intensity factor is given as

$$K_{Ic}^s = \frac{3P_u S}{2bd^2} \sqrt{\pi a_e} F(\alpha_e) \quad (21)$$

$$F(\alpha) = \frac{1}{\sqrt{\pi}} \frac{1.99 - \alpha(1-\alpha)(2.15 - 3.93\alpha + 2.7\alpha^2)}{(1+2\alpha)(1-\alpha)^{3/2}}, \quad S/d = 4 \quad (22)$$

where P_u is the maximum load. The critical crack-tip opening displacement is given by

$$CTOD_c = \frac{6P_u S a_e}{bd^2 E_c} V_1(\alpha_e) \{(1-\beta^2) + (-1.149\alpha_e + 1.081)(\beta - \beta^2)\}^{1/2} \quad (23)$$

in which $\beta = a_0/a_e$

Appendix B

The calculation of the fracture parameters in ECM

The modulus of elasticity is calculated as follows

$$E = \frac{P_i}{4b\delta_i} \left(\frac{S}{d(1-\alpha_0)} \right)^3 \left(1 + \frac{5q}{8P_i} \right) \lambda \quad (24)$$

where P_i , δ_i are measured at about 50% peak load location on the initial ascending portion of the load-deflection curve and q is the self-weight of the specimens. λ which can be determined from finite element calculations is a correction factor relating deflections of a notched to an unnotched specimen and given by

$$\lambda = \eta_1 \exp \left[\eta_2 \left(\frac{a_0}{d} \right)^2 + \eta_3 \left(\frac{S}{d} \right)^2 + \eta_4 \left(\frac{a_0}{d} \right) \left(\frac{S}{d} \right) + \eta_5 \left(\frac{S}{d} \right)^3 \right] \quad (25)$$

in which $\eta_1 = 1.379$, $\eta_2 = -1.463$, $\eta_3 = -0.036$, $\eta_4 = -0.201$ and $\eta_5 = 0.004$. The effective crack length is calculated by trial and error method as follows

$$\frac{a_e}{d} = 1 - \left[\frac{P_u}{4bd^3 \delta_u E_c} \left(1 + \frac{5q}{8P_u} \right) \lambda \right]^{1/3} \quad (26)$$

where δ_u is the displacement at the peak load. a_e in Eq. (26) can be also determined by the regression formula from

$$\frac{a_e}{d} = \gamma_1 \left(\frac{\sigma_u}{E_c} \right)^{\gamma_2} \left(\frac{a_0}{d} \right)^{\gamma_3} \left(1 + \frac{d_{\max}}{d} \right)^{\gamma_4} \quad (27)$$

where $\sigma_u = 6M_u/(bd^2)$, $M_u = (P_u + q/2)S/4$ and $\gamma_1 = 0.088 \pm 0.004$, $\gamma_2 = -0.208 \pm 0.010$, $\gamma_3 = 0.451 \pm 0.013$ and $\gamma_4 = 1.653 \pm 0.109$. The critical stress intensity factor, K_{Ic}^e according to the ECM can be estimated the similar to TPM from Eq. (21) and Eq. (22).

Appendix C

The calculation of the fracture parameters in SEM

The critical stress intensity factor can be determined for infinite large specimen as follows

$$K_{Ic} = B \sqrt{d_0 g(\alpha_0)} \quad (28)$$

in which the function g is the nondimensional energy release rate calculated according to LEFM given by

$$g(\alpha) = \left(\frac{L}{d} \right)^2 \pi \alpha [1.5F(\alpha)]^2 \quad (29)$$

$$F(\alpha) = \frac{1.0 - 2.5\alpha + 4.49\alpha^2 - 3.98\alpha^3 + 1.33\alpha^4}{(1 - \alpha)^{3/2}}, \quad S/d = 2.5 \quad (30)$$

The fracture energy is calculated the similar to LEFM as follows

$$G_f = \frac{K_{Ic}^2}{E_c} \quad (31)$$

The effective crack length can be determined given by

$$c_f = d_0 \frac{g(\alpha_0)}{g'(\alpha_0)} \quad (32)$$

where $g'(\alpha) = dg(\alpha)/d\alpha$. Eq. (32) is only valid for $g'(\alpha_0) > 0$. The critical crack tip opening displacement is calculated as follows

$$\delta_c = \sqrt{\frac{32G_f c_f}{\pi E_c}} \quad (33)$$